THE JOURNAL OF PHYSICAL CHEMISTRY B
A JOURNAL OF THE AMERICAN CHEMICAL SOCIETY

pubs.acs.org/JPCB

Article

Computation of Shear Viscosity by a Consistent Method in Equilibrium Molecular Dynamics Simulations: Applications to 1-Decene Oligomers

Luís Fernando Mercier Franco* and Abbas Firoozabadi

Cite This: https://doi.org/10.1021/acs.jpcb.3c04994

Read Online

ACCESS | Metrics & More | Article Recommendations | Supporting Information

ABSTRACT: Accurate computation of shear viscosity is fundamental for describing fluid flow and designing and developing new processes. Poly-α-olefins (PAO's), particularly from 1-decene, have been applied to a variety of industrial processes. Recently, these molecules have been applied as carbon dioxide thickeners, enhancing carbon dioxide viscosity, which is important in carbon dioxide injection, either for enhanced oil recovery or carbon sequestration in geological formations. For these applications, knowledge of the pure oligomer viscosity is crucial to design and operate the oligomer upstream pipelines before mixing them with carbon dioxide. Using Green−Kubo formalism with equilibrium molecular dynamics simulations, two methods are presented in the literature to generate the traceless, symmetric pressure tensor. In this work, we show that these two methods provide different values of shear viscosity, from the analysis of how the diagonal components of the traceless, symmetric pressure tensor are computed in each method. Then, we examine the consistency and correctness of each method: one is found to be consistent. The other is corrected by scaling the fluctuations of the diagonal components. Shear viscosities of supercritical carbon dioxide, vapor and liquid *n*-pentane, and liquid *n*-decane are computed to illustrate the analysis. We also apply the consistent method to compute the viscosity of 1-decene oligomers, including for the first time larger-than-dimer oligomers (trimer, tetramer, hexamer, and decamer).

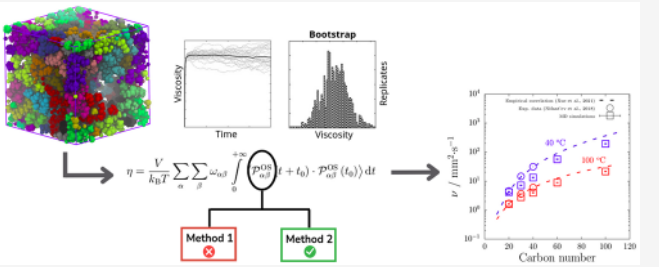

INTRODUCTION

Shear viscosity is a fundamental property in fluid dynamics.[1] A considerable number of applications depend on accurate measurement or prediction of viscosity. Poly-α-olefins (PAO's) comprise a family of branched saturated hydrocarbons with low molecular weight. They are synthesized through the catalytic oligomerization of linear α-olefins.[2] Their primary application as a lubricating base oil covers a broad spectrum of industries from automobile to aerospace, and food.[3,4]

Another interesting recent application of poly-α-olefin oligomers, particularly those based on 1-decene, is in the ability to viscosify carbon dioxide. Carbon dioxide injection in hydrocarbon reservoirs has a dual merit: enhance the oil recovery, and sequestrate carbon in geological formations.[5] The low viscosity of carbon dioxide presents a significant challenge in controlling its mobility within mineral rocks. A promising alternative is viscosifying carbon dioxide by adding chemical thickeners. 1-Decene oligomers are good candidates. Recently, these molecules have been proven to significantly increase carbon dioxide viscosity, both experimentally[6,7] and through Dissipative Particle Dynamics simulations.[8]

To turn such an alternative into a viable technology in carbon dioxide sequestration, an accurate prediction of the viscosity of the pure oligomers is a crucial step. The mixing process between carbon dioxide and the viscosifier requires pure viscosifier transport through flowlines. The accurate prediction of the viscosifier shear viscosity is paramount to design and has a significant impact on the economic analysis of the pumping and transport processes.

Predicting the viscosity remains a challenging task. Classical molecular dynamics simulations have been used to predict transport properties, including shear viscosity, for a variety of systems. The main approaches are Non-Equilibrium Molecular Dynamics (NEMD) and Equilibrium Molecular Dynamics (EMD).[9] The NEMD consists of applying a shear to the simulation box, and from the velocity profiles at the steady-state, the shear viscosity can be determined. This approach is intuitive, and one needs to be careful in selecting appropriate parameters such as system size, velocity gradient, and time to achieve steady-state. Shear viscosity can also be computed from EMD. Two equivalent approaches are used: Green−Kubo[10,11] (GK) and Einstein-Helfand[12] (EH). GK is based on

Received: July 25, 2023
Revised: October 18, 2023
Accepted: October 23, 2023

the time integral of the stress autocorrelation function, and EH is based on the mean-square displacement of a certain coordinate of the center of momentum of another coordinate. This work is focused on the application of the GK method.

Shear viscosity is related to the off-diagonal components of the pressure tensor. Because the pressure tensor is symmetric, this results in three independent values per time step. To improve statistics, it is customary to use the information from the diagonal components and to construct a traceless, symmetric pressure tensor. Then, one can compute six independent stress autocorrelation functions. This approach has been demonstrated by Daivis and Evans[13] by writing the invariant of the shear viscosity tensor.

Green−Kubo relation for shear viscosity calculations, taking into account all six independent components, is given by the following expression:

$$\eta = \frac{V}{k_B T} \sum_{\alpha} \sum_{\beta} \omega_{\alpha\beta} \int_0^{+\infty} \langle \mathcal{P}^{OS}_{\alpha\beta}(t + t_0) \cdot \mathcal{P}^{OS}_{\alpha\beta}(t_0) \rangle \, dt \tag{1}$$

where η is the shear viscosity, V is the simulation box volume, k_B is the Boltzmann constant, T is the absolute temperature, $\mathcal{P}^{OS}_{\alpha\beta}$ is the $\alpha\beta$ component of the traceless, symmetric pressure tensor, t is time, and $\omega_{\alpha\beta}$ is the weight factors, which may vary for different methods.

At least two methods to generate a traceless symmetric pressure tensor can be followed. Method 1 is based on subtracting one-third of the symmetric pressure tensor trace from each of its diagonal components:[14−19]

$$\mathcal{P}^{OS,(1)}_{\alpha\beta} = \frac{\mathcal{P}_{\alpha\beta} + \mathcal{P}_{\beta\alpha}}{2} - \frac{\delta_{\alpha\beta}}{3} \sum_{\gamma} \mathcal{P}_{\gamma\gamma} \tag{2}$$

where $\delta_{\alpha\beta}$ is the Kronecker delta. The superscript "(1)" in Equation 2 stands for Method 1.

The weight factors usually suggested to be used in the first method read as

$$\omega^{(1)}_{\alpha\beta} = \frac{1}{10}\left(1 + \frac{\delta_{\alpha\beta}}{3}\right) \tag{3}$$

Some authors[14] have applied Method 1 with different weight factors: $\omega_{\alpha\beta} = 1/9$. For the purpose of the analysis conducted here, we will consider only Method 1 with the weight factors given by eq 3.

In Method 2, the traceless, symmetric pressure tensor is computed according to the following equation:

$$\mathcal{P}^{OS,(2)}_{\alpha\beta} = \begin{cases} \dfrac{\mathcal{P}_{\alpha\alpha} - \mathcal{P}_{\beta\beta}}{2}, & \text{if } (\alpha, \beta) = (x, y), (y, z), \text{or } (z, x) \\ \dfrac{\mathcal{P}_{\alpha\beta} + \mathcal{P}_{\beta\alpha}}{2}, & \text{if } \alpha \neq \beta. \end{cases} \tag{4}$$

Superscript "(2)" in eq 4 stands for Method 2.

This second method has been applied in the literature,[20−22] with a minor difference in the $\mathcal{P}^{OS}_{zz}$. Some authors use: $\mathcal{P}^{S}_{zz} = 0.5(\mathcal{P}_{xx} - \mathcal{P}_{zz})$, which is still a symmetric pressure tensor, but not traceless. We apply the second method computing $\mathcal{P}^{OS}_{zz} = 0.5(\mathcal{P}_{zz} - \mathcal{P}_{xx})$, to properly get a traceless, symmetric pressure tensor.

In this case, the weight factors usually suggested can be expressed as

$$\omega^{(2)}_{\alpha\beta} = \frac{(1 + \delta_{\alpha\beta})}{12} \tag{5}$$

If one considers only off-diagonal components of the pressure tensor in the Green−Kubo calculation, then the two methods are exactly the same.

To examine whether the two methods yield the same results, we compute shear viscosities for supercritical carbon dioxide, vapor and liquid *n*-pentane, and liquid *n*-decane, via classical equilibrium molecular dynamics simulations. After selecting the method, we computed the shear viscosity of 1-decene oligomers ranging from the dimer to the decamer at two different temperatures.

METHODS

Force Fields. Two classical atomistic force fields for carbon dioxide are used: TraPPE[23] and EPM2;[24] both are known to provide good estimates of shear viscosity.[25] Both force fields are treated here with rigid bonds, and the intermolecular potential is given by a Lennard-Jones potential summed to a Coulomb potential. To maintain the linearity of carbon dioxide, the total molecular weight is split in two virtual sites constrained at a distance that gives the same moment of inertia. For Lennard-Jones crossed parameters, Lorentz−Berthelot combining rules are used for TraPPE, and geometrical combining rules are used for EPM2.

For liquid *n*-pentane, two force fields are used: TraPPE with a united atom description and OPLS (Optimized Potentials for Liquid Simulations) with explicit hydrogens. For vapor *n*-pentane, only calculations with TraPPE are performed, since OPLS is optimized for liquid simulations. For TraPPE, all bonds are treated as rigid. For OPLS, only C−H bonds are constrained. TraPPE intermolecular potential is given by a Lennard-Jones potential. OPLS intermolecular potential is given by a Lennard-Jones potential summed to a Coulomb potential. For Lennard-Jones cross parameters, Lorentz−Berthelot combining rules are used for TraPPE, and geometrical combining rules are used for OPLS.

For liquid *n*-decane, as well as for 1-decene oligomers (dimer, trimer, tetramer, hexamer, and decamer), L-OPLS all-atoms[26,27] force field is employed. This force field has been successfully applied to compute the shear viscosity of 1-decene dimer[27] and of the saturated 1-decene trimer.[28] Only C−H bonds are constrained. The intermolecular potential is given by a Lennard-Jones potential summed to a Coulomb potential. For Lennard-Jones crossed parameters, geometrical combining rules are used for OPLS.

The potential parameters for all force fields are provided in the Supporting Information (Tables S1 to S12).

Molecular Dynamics Simulations. All simulations are performed in Gromacs[29] 2018.3 (for carbon dioxide) and 2020.1 (for all the other systems). The leapfrog algorithm is used to integrate Newton's equations of motion with a time step of 1 fs for carbon dioxide and *n*-pentane and 2 fs for *n*-decane, and the 1-decene oligomers. Periodic boundary conditions are applied to all directions. Electrostatic interactions are computed using PME.[30] The neighboring list is updated every 10 steps. For TraPPE and EPM2, analytical long-tail corrections for the truncated Lennard-Jones potential are applied to both energy and pressure.[9] Following the prescription for L-OPLS force field, a switch function between 1.1 and 1.3 nm is used to compute the Lennard-Jones potential, and analytical long-tail corrections are applied to

https://doi.org/10.1021/acs.jpcb.3c04994
J. Phys. Chem. B XXXX, XXX, XXX−XXX

Table 1. Number of Molecules and Dimensions of the Initial Configurations for the MD Simulations for Each Compound

compound	force field	phase	number of molecules	dimensions
carbon dioxide	TraPPE and EPM2	supercritical	500	$4 \times 4 \times 4$ nm^3
n-pentane	TraPPE	vapor	400	$12.4 \times 12.4 \times 12.4$ nm^3
		liquid	400	$4.3 \times 4.3 \times 4.3$ nm^3
	OPLS	liquid	120	$3 \times 3 \times 3$ nm^3
n-decane	L-OPLS	liquid	80	$5 \times 5 \times 5$ nm^3
1-decene	L-OPLS	liquid	80	$5 \times 5 \times 5$ nm^3
1-decene dimer	L-OPLS	liquid	67	$5 \times 5 \times 5$ nm^3
1-decene trimer	L-OPLS	liquid	45	$4 \times 4 \times 4$ nm^3
1-decene tetramer	L-OPLS	liquid	34	$4 \times 4 \times 4$ nm^3
1-decene hexamer	L-OPLS	liquid	60	$8 \times 8 \times 8$ nm^3
1-decene decamer	L-OPLS	liquid	40	$8 \times 8 \times 8$ nm^3

both energy and pressure.[9] The LINCS algorithm is employed to constrain all bonds for TraPPE and EPM2, and only C−H bonds for OPLS.

Initial Configurations. The initial configurations for all the systems are built in Packmol[31] with a tolerance of 2.0 Å. After generating initial configurations, all systems are subjected to energy minimization using the steepest descent method, assuming convergence when the maximum force is smaller than 1000 kJ·mol^{-1}·nm^{-1}. Table 1 presents the number of molecules and the dimensions of the initial cubic box for each MD simulation.

Equilibration and Production Runs. For carbon dioxide and *n*-pentane, after energy minimization, the systems are equilibrated in the isobaric−isothermal ensemble. For *n*-decane and all the 1-decene oligomers, after energy minimization and before the equilibration runs, the systems are subjected to simulated annealing in the isobaric−isothermal ensemble at time 0, simulations begin at 298.15 K, which is linearly raised to a maximum of 750 K at 0.5 ns, and finally linearly dropped to the target temperature at 1 ns. This step ensures that the system can relax to the correct density at the specified temperature and pressure.

After the annealing process and energy minimization for carbon dioxide and *n*-pentane, two equilibration stages are conducted. The first equilibration is carried out in the isobaric−isothermal ensemble applying the Berendsen thermostat[32] with a coupling parameter of 1 ps, and the Berendsen barostat[32] with a coupling parameter of 1 ps and compressibility of 4.5×10^{-5} bar^{-1}. The second equilibration stage is carried out in the canonical ensemble, with the Nosé−Hoover thermostat[33,34] and a coupling parameter of 1 ps. The production runs are conducted in the canonical ensemble with the Nosé−Hoover thermostat[33,34] and a coupling parameter of 1 ps. Pressure tensor components are sampled every 5 fs.

Table 2 presents the total times for each one of the runs for each compound.

Uncertainty Estimation in Shear Viscosity Calculations. In shear viscosity calculations, multiple independent trajectories are run with different seeds for initializing velocities (with values ranging from 1001 to 1040, depending on the total number of independent trajectories). Green−Kubo relation is applied to each of these independent trajectories. A bootstrap method[16,35] is used to quantify the uncertainty and compute the average shear viscosity. A number of replicates out of the total number of independent trajectories are randomly selected with replacement. The shear viscosity as a function of time is averaged over these replicates, and a double-exponential function integrated over time[21,36] is fitted to the resulting averaged function:

Table 2. Run Time (In Nanoseconds) For Each MD Stage: Annealing, Equilibration, And Production for Each Compound

	annealing	equilibration		production
compound	NPT	NPT	NVT	NVT
carbon dioxide		4	1	3
n-pentane		4	1	4
n-decane	2	8	2	6
1-decene	2	1	1	4
1-decene dimer	2	1	1	4
1-decene trimer	2	1	1	4
1-decene tetramer	2	1	1	4
1-decene hexamer	2	4	1	9
1-decene decamer	2	4	1	9

$$\eta(t) = A\alpha\tau_1(1 - e^{-t/\tau_1}) + A(1 - \alpha)\tau_2(1 - e^{-t/\tau_2}) \quad (6)$$

where A, α, τ_1, and τ_2 are fitting parameters.

The fitting is carried out based on the Nelder−Mead algorithm[37] minimizing the least-squares deviation. A weight of $1/t^b$ is used, following the time decomposition method,[38] in which the standard deviation is fitted among the replicates as a function of time up to a cutoff time to a power law, which can be linearized as follows:

$$\ln \sigma(t) = a + b \ln t \quad (7)$$

where a and b are fitting parameters.

The infinity-time limit value is taken from the time-integrated, double-exponential function $\eta(t \to +\infty) = A\alpha\tau_1 + A(1 - \alpha)\tau_2$. The process of selecting random replicates with replacement is repeated several times to generate a histogram. For a confidence level of 95%, the critical value of t for a two-tailed test is considered 1.962 for 1000 degrees of freedom and 1.984 for 100 degrees of freedom. Degrees of freedom are defined as the number of random selections (with replacement) in the bootstrap method minus 1. The final shear viscosity and its uncertainty is given by

$$\eta = \langle\eta\rangle \pm t \times \frac{\sigma}{\sqrt{n}} \quad (8)$$

where $\langle\eta\rangle$ is the average value of shear viscosity computed from the values generated in the bootstrap method, $n = 1001$ for 1000 degrees of freedom or 101 for 100 degrees of freedom, and σ is the standard deviation.

https://doi.org/10.1021/acs.jpcb.3c04994
J. Phys. Chem. B XXXX, XXX, XXX−XXX

Table 3 presents the number of independent trajectories, the number of replicates, the cutoff time, and the degrees of freedom for each compound.

Table 3. Number of Independent Trajectories, Number of Replicates, Cutoff Time, and Degrees of Freedom for Each Compound

compound	independent trajectories	replicates	cutoff time (ps)	degrees of freedom
carbon dioxide	30	20	20	1000
n-pentane	30	30	50	100
n-decane (260, 300, and 340 K)	30	30	500	100
n-decane (380 K)	30	30	150	100
1-decene	20	20	150	100
1-decene dimer	20	20	500	100
1-decene trimer	20	20	500	100
1-decene tetramer	20	20	2000	100
1-decene hexamer	40	40	4500	100
1-decene decamer	40	40	4500	100

RESULTS AND DISCUSSION

Consistent Method to Compute Viscosity via EMD Simulations. Figure 1 presents the shear viscosity computed

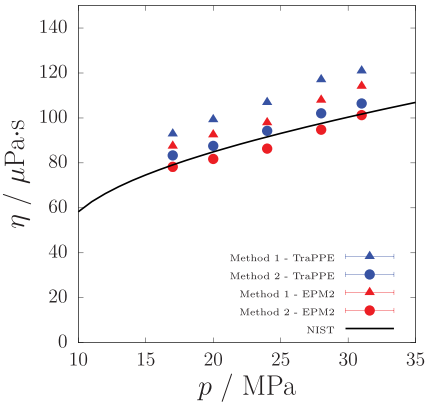

Figure 1. Shear viscosity of supercritical carbon dioxide at 308 K versus pressure. Continuous line, NIST data.[39] Blue triangles are MD simulations with the TraPPE force field in Method 1. Red triangles, MD simulations with the EPM2 force field in Method 1. Blue circles, MD simulations with the TraPPE force field in Method 2. Red circles, MD simulations with the EPM2 force field in Method 2. The uncertainties are smaller than the symbol sizes. They are reported in Table S13.

using Methods 1 and 2 for the traceless, symmetric pressure tensor from the two force fields for supercritical carbon dioxide at 308 K as a function of pressure. The shear viscosity computed using Method 1 from the two force fields is consistently overestimated in comparison with that computed using Method 2. The result from Method 2 is in better agreement with NIST data.[39]

Aimoli et al.[25] used the Green−Kubo formalism considering only off-diagonal components of the pressure tensor to compute the shear viscosity of supercritical CO_2. They obtained an absolute average relative deviation (AARD) of 4.69% with EPM2 and 7.32% with TraPPE. In our calculations, we obtain using Method 2 an AARD of 2.73% with EPM2 and 4.17% with TraPPE. Using Method 1, we obtain 9.86% with EPM2 and 18.0% with TraPPE. These results show an agreement between Method 2, as computed in this work, and the values computed by Aimoli et al.[25] using only the off-diagonal components.

Figure 2 presents the computed shear viscosity for *n*-pentane under subcritical conditions (vapor and liquid) as well as NIST

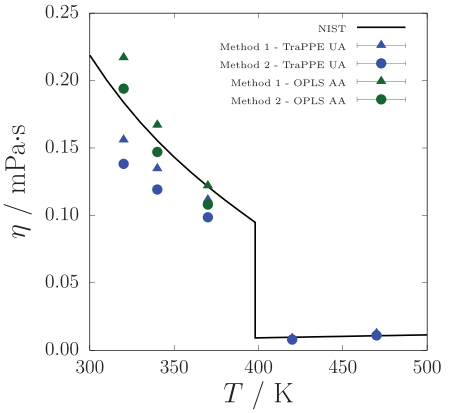

Figure 2. Shear viscosity of *n*-pentane at 10 bar versus temperature. Continuous line, NIST data.[39] Blue triangles are MD simulations with the TraPPE-UA force field in Method 1. Green triangles are MD simulations with the OPLS-AA force field in Method 1. Blue circles, MD simulations with the TraPPE-UA force field in Method 2. Green circles, MD simulations with the OPLS-AA force field in Method 2. The uncertainties are reported in Table S14.

data. Two force fields are used for the liquid phase: TraPPE united atom and OPLS. For the vapor phase, only TraPPE is used, because OPLS is optimized for liquid simulations. A persistent difference between Methods 1 and 2 is seen. Method 1 consistently gives shear viscosity higher than Method 2.

Figure 3 presents the computed shear viscosity for liquid *n*-decane as a function of temperature, as well as NIST data. A

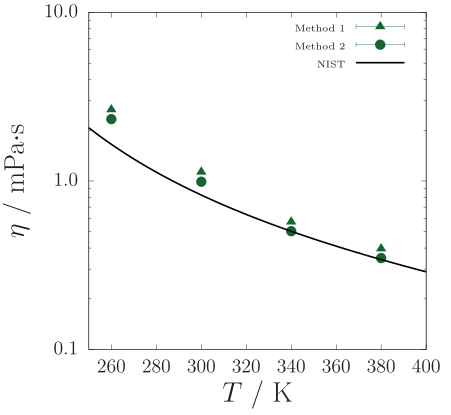

Figure 3. Shear viscosity of liquid *n*-decane at 1 bar versus temperature. Continuous line, NIST data.[39] Green triangles are MD simulations with the L-OPLS-AA force field in Method 1. Blue circles are MD simulations with the L-OPLS-AA force field in Method 2. The uncertainties are reported in Table S16.

single force field is used (L-OPLS-AA). Method 1 gives higher shear viscosity than Method 2.

Figure 4 presents the ratio of shear viscosities computed using Method 2 and Method 1 as a function of pressure.

https://doi.org/10.1021/acs.jpcb.3c04994
J. Phys. Chem. B XXXX, XXX, XXX−XXX

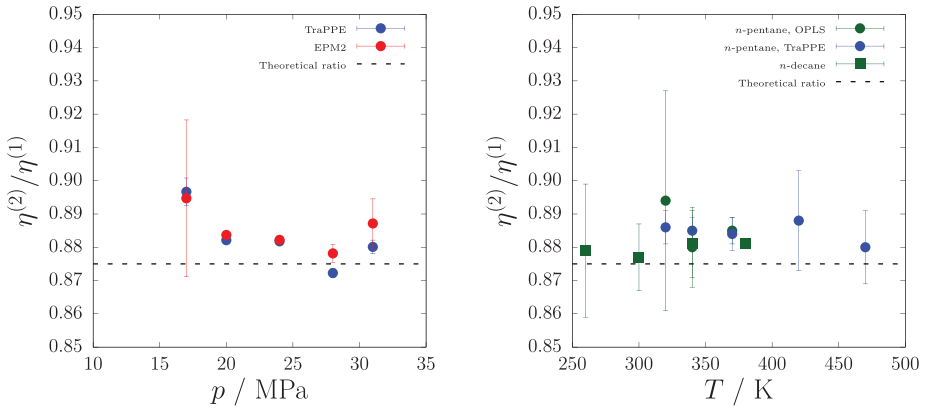

Figure 4. Ratio of the two shear viscosities computed using Method 2 and Method 1. (Left) Ratio for carbon dioxide versus pressure at 308 K. Blue circles, MD simulations with the TraPPE force field. Red circles, MD simulations with the EPM2 force field. The dashed black line corresponds to the theoretical ratio proposed in this work. (Right) Circles, *n*-pentane at 10 bar, and squares, *n*-decane at 1 bar versus temperature. Blue symbols are MD simulations with the TraPPE force field. Green symbols, MD simulations with the OPLS force field.

Interestingly, this ratio seems to be constant regardless of the force field and the thermodynamic condition.

One possible explanation for this inconsistency between the two methods is the way they are formulated. In Method 1, to build each diagonal component of the traceless, symmetric pressure tensor, all three diagonal components of the pressure tensor are used, as opposed to only two employed in Method 2. Because each pressure tensor component has its own fluctuation, when propagated, the fluctuations of the diagonal components of the resulting traceless, symmetric pressure tensor are larger in Method 1 than in Method 2. Moreover, the off-diagonal components are constructed by using only two pressure tensor components. Therefore, in method 2, all traceless, symmetric pressure tensor components have fluctuations at the same order of magnitude, whereas for Method 1, the diagonal components have larger fluctuations. These larger fluctuations are manifested in the significant increase in the stress autocorrelation function (SAFC) as shown in Figure 5, comparing the *xx* component SAFC's computed in both methods with a off-diagonal component SAFC.

To prove our reasoning, we estimate the fluctuations of the diagonal components in both methods. The traceless, symmetric pressure tensor covariance matrix can be computed as follows:

$$\boldsymbol{\Sigma}_{\mathbf{P}^{\mathrm{OS}}} = \mathbf{J}\boldsymbol{\Sigma}_{\mathbf{P}}\mathbf{J}^{\mathrm{T}} \tag{9}$$

where $\Sigma_{\mathbf{P}^{\mathrm{OS}}}$ is the traceless, symmetric pressure tensor covariance, $\mathbf{J}$ is the Jacobian matrix, and $\boldsymbol{\Sigma}_{\mathbf{P}}$ is the pressure tensor covariance.

Since in both methods (1 and 2) the traceless, symmetric pressure tensor components are expressed as linear combinations of the components of the pressure tensor:

$$\mathcal{P}^{\mathrm{OS}}_{\alpha\beta} = \sum_i \sum_j a_{ij}\mathcal{P}_{ij} \tag{10}$$

where a_{ij} are the linear combination coefficients. The coefficients of the covariance matrix in eq 9 reduce to

$$\sigma^2_{\mathcal{P}^{\mathrm{OS}}_{\alpha\beta}} = \sum_i \sum_j \sum_k \sum_l a_{ij}a_{kl}\rho_{ijkl}\sigma_{\mathcal{P}_{ij}}\sigma_{\mathcal{P}_{kl}} \tag{11}$$

where ρ_{ijkl} is the correlation coefficient.

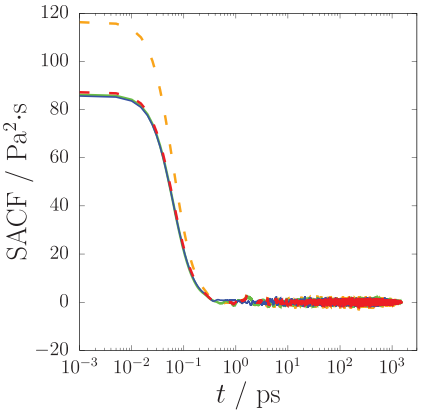

Figure 5. Stress autocorrelation function (SACF) versus time for supercritical carbon dioxide at 308 K and 17 MPa, computed with classical equilibrium molecular dynamics simulations with the EPM2 force field. Continuous green line, SACF computed using $\mathcal{P}^{\mathrm{OS}}_{xx}$ with Method 2. Dashed orange line, SACF computed using $\mathcal{P}^{\mathrm{OS}}_{xx}$ with Method 1. Continuous blue line, SACF computed using $\mathcal{P}^{\mathrm{OS}}_{xy}$. Dashed red line, SACF computed using $\mathcal{P}^{\mathrm{OS}}_{xx}$ with Method 1, scaled by 3/4, which is the ratio of the variances of methods 2 and 1: eq 18.

The differences between Method 1 and Method 2 lie on the diagonal components of the traceless, symmetric pressure tensor, which, from eq 11, can be written as

$$\sigma^2_{\mathcal{P}^{\mathrm{OS}}_{\alpha\alpha}} = \sum_i \sum_k a_{ii}a_{kk}\rho_{iikk}\sigma_{\mathcal{P}_{ii}}\sigma_{\mathcal{P}_{kk}} \tag{12}$$

The pressure tensor components are statistically independent, which results in $\rho_{iikk} \approx \delta_{ik}$:

$$\sigma^2_{\mathcal{P}^{\mathrm{OS}}_{\alpha\alpha}} = \sum_i \sum_k a_{ii}a_{kk}\delta_{ik}\sigma_{\mathcal{P}_{ii}}\sigma_{\mathcal{P}_{kk}} \tag{13}$$

and, therefore

$$\sigma^2_{\mathcal{P}^{\mathrm{OS}}_{\alpha\alpha}} = \sum_i a_{ii}^2\sigma^2_{\mathcal{P}_{ii}} \tag{14}$$

For Method 1, eq 14 becomes

$$\sigma^2_{\mathcal{P}^{\mathrm{OS},(1)}_{\alpha\alpha}} = \left(\frac{2}{3}\right)^2\sigma^2_{\mathcal{P}_{\alpha\alpha}} + \left(\frac{1}{3}\right)^2\sigma^2_{\mathcal{P}_{\beta\beta}} + \left(\frac{1}{3}\right)^2\sigma^2_{\mathcal{P}_{\gamma\gamma}} \tag{15}$$

https://doi.org/10.1021/acs.jpcb.3c04994
J. Phys. Chem. B XXXX, XXX, XXX−XXX

For Method 2, eq 14 becomes

$$\sigma^2_{\mathcal{P}^{\mathrm{OS},(2)}_{\alpha\alpha}} = \left(\frac{1}{2}\right)^2 \sigma^2_{\mathcal{P}_{\alpha\alpha}} + \left(\frac{1}{2}\right)^2 \sigma^2_{\mathcal{P}_{\beta\beta}} \tag{16}$$

For an isotropic system, the variances of the diagonal components of the pressure tensor should be very close to each other:

$$\sigma^2_{\mathcal{P}_{\alpha\alpha}} \approx \sigma^2_{\mathcal{P}_{\beta\beta}} \approx \sigma^2_{\mathcal{P}_{\gamma\gamma}} \tag{17}$$

As a consequence, the ratio of the variance of the diagonal components between the two methods is

$$\frac{\sigma^2_{\mathcal{P}^{\mathrm{OS},(2)}_{\alpha\alpha}}}{\sigma^2_{\mathcal{P}^{\mathrm{OS},(1)}_{\alpha\alpha}}} \approx \frac{\frac{1}{2}\sigma^2_{\mathcal{P}_{\alpha\alpha}}}{\frac{2}{3}\sigma^2_{\mathcal{P}_{\alpha\alpha}}} = \frac{3}{4} \tag{18}$$

When multiplied by the ratio calculated in Equation 18, the stress autocorrelation function (SACF) computed in Method 1 perfectly matches the SACF computed in Method 2 and with the off-diagonal SACF. This is shown in Figure 5 for supercritical carbon dioxide at 308 K and 17 MPa. The ratio expressed in eq 18 suggests a scaling factor for the larger fluctuations by the diagonal components of the traceless, symmetric pressure tensor calculated in Method 1.

Direct comparison of results from Methods 1 and 2 and experimental data may not provide clear guidance due to the force field effect in representing thermophysical properties. The terms that naturally contribute to shear viscosity are the off-diagonal terms of the pressure tensor. The diagonal terms can be used to improve the statistics. For that purpose, the resulting stress-autocorrelation function should match those computed with the off-diagonal terms. This indeed is a feature of Method 2, but not of Method 1 (see Figure 5). The stress-autocorrelation functions calculated via Method 1 using the diagonal terms are overestimated.

In Table S15, we present the comparison, for OPLS *n*-pentane at 370 K and 10 bar, from Method 1, Method 2, and the calculations using only the off-diagonal elements of the pressure tensor. Although Method 1 gives a closer value with respect to the NIST data, Method 2 agrees with the off-diagonal calculations. Method 2 is the correct and consistent way of improving statistics (which is indeed verified analyzing the estimated uncertainties), and the differences between its results and NIST data is directly related to the inaccuracy of the selected force field.

Including the ratio of the variances of methods 2 and 1 (Equation 18 corrects the shear viscosities computed via Method 1. The traceless, symmetric pressure tensor has 6 independent components. This implies 6 independent stress-autocorrelation functions. Assuming an *a priori* weight of 1/6, the weights of the stress-autocorrelation functions, computed with diagonal components, should be corrected by multiplying them by the ratio of the variances of methods 2 and 1, which is 3/4, eq 18. This means a 1/8 weight for diagonal terms and 1/12 weight for off-diagonal terms, considering the three pairs of independent off-diagonal terms. Incorporating this correction, the weight factors for the modified Method 1 may be expressed as

$$\omega^{(1)}_{\alpha\beta} = \frac{(2 + \delta_{\alpha\beta})}{24} \tag{19}$$

In the original Method 1 and Method 2, the summation of the weight factors is one. For the modified Method 1 proposed in this work, the sum over all weight factors is

$$\sum_\alpha \sum_\beta \omega^{(1)}_{\alpha\beta} = \frac{7}{8} \tag{20}$$

Interestingly, the value of this summation, Equation 20, agrees with the ratio of the shear viscosities computed with Method 2 and the original Method 1, as shown in Figure 2. This can be proven by comparing the invariant term in Green−Kubo formalism. In the original Method 1, the shear viscosity is computed by

$$\eta^{(1)} = \frac{V}{k_B T} \sum_\alpha \sum_\beta \omega^{(1)}_{\alpha\beta} \int_0^{+\infty} \langle \mathcal{P}^{\mathrm{OS}}_{\alpha\beta}(t + t_0) \cdot \mathcal{P}^{\mathrm{OS}}_{\alpha\beta}(t_0) \rangle \, \mathrm{d}t \tag{21}$$

where $\eta^{(1)}$ is the shear viscosity computed using the original Method 1, and $\omega^{(1)}_{\alpha\beta}$ is the weight factors of the original Method 1, as shown in eq 3.

The shear viscosity from the modified Method 1 proposed in this work can be computed as

$$\eta^{(1*)} = \frac{V}{k_B T} \sum_\alpha \sum_\beta \omega^{(1*)}_{\alpha\beta} \int_0^{+\infty} \langle \mathcal{P}^{\mathrm{OS}}_{\alpha\beta}(t + t_0) \cdot \mathcal{P}^{\mathrm{OS}}_{\alpha\beta}(t_0) \rangle \, \mathrm{d}t \tag{22}$$

where $\eta^{(1*)}$ is the shear viscosity computed using the modified Method 1, and $\omega^{(1*)}_{\alpha\beta}$ is the weight factors of the modified Method 1, as shown in eq 19.

The modified Method 1 must be consistent with Method 2. The shear viscosity computed with modified Method 1 is expected to be equal to the shear viscosity computed with modified Method 2. The ratio of the shear viscosities computed from the modified Method 1 proposed in this work and the original Method 1 is then

$$\frac{\eta^{(2)}}{\eta^{(1)}} = \frac{\eta^{(1*)}}{\eta^{(1)}} = \frac{\sum_\alpha \sum_\beta \omega^{(1*)}_{\alpha\beta}}{\sum_\alpha \sum_\beta \omega^{(1)}_{\alpha\beta}} = \frac{7}{8} \tag{23}$$

In Figure 5, this theoretical ratio is drawn as a dashed line and agrees very well with the computed ratios. A modified Method 1, as derived in this work, can be implemented either by applying the weight factors in eq 19 or by applying the factor calculated in eq 23 directly to the final shear viscosity. Both the correction factor and weight factors in eq 19 are only theoretical approximations based on the assumptions that the diagonal pressure tensor components are statistically independent and that the variance is the same for all diagonal pressure tensor components. A more rigorous correction factor would require careful evaluation of these two assumptions. We suggest the use of Method 2 in the calculation of the traceless, symmetric pressure tensor components. The approach is straightforward and is free from *a fortiori* correction factors. We use Method 2 to compute the shear viscosity of 1-decene oligomers.

Viscosity of 1-Decene Oligomers. Molecular dynamics simulations have been used to compute the shear viscosity of α-olefins oligomers (dimers and trimers) for more than two decades. Kioupis and Maginn[40,41] have computed via non-equilibrium molecular dynamics simulations the shear viscosity of the saturated 1-hexene trimer. Using nonequilibrium molecular dynamics simulations, Mathas et al.[27] have

https://doi.org/10.1021/acs.jpcb.3c04994
J. Phys. Chem. B XXXX, XXX, XXX−XXX

computed the shear viscosity of 1-decene dimer, applying the L-OPLS-AA force field. Ravikumar et al.[42] have also applied L-OPLS-AA to compute the shear viscosity of 1-decene dimer, with good agreement with experimental data for PAO-2.[43] More recently, Schmitt et al.[28] have computed the shear viscosity of the saturated 1-decene trimer using several different force fields.

Before computing the shear viscosity of 1-decene oligomers, the density and shear viscosity of the monomer are computed and compared to experimental data. Figure 6 presents the

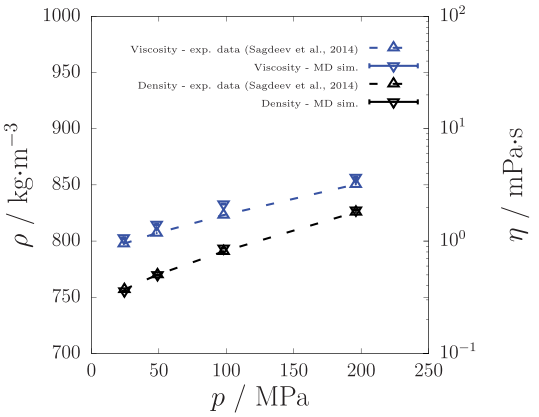

Figure 6. Density (left *y* axis) and shear viscosity (right *y* axis) versus pressure for 1-decene at 298.15 K. Black up-pointing triangle, experimental density data.[44] Black down-pointing triangle, density from MD simulations. Blue up-pointing triangle, experimental shear viscosity data.[44] Blue down-pointing triangle, shear viscosity from MD simulations. The uncertainties are reported in Table S17.

density and shear viscosity of 1-decene versus pressure at 298.15 K. The agreement between the molecular dynamics simulations and experimental data is very good. The shear viscosity is slightly overestimated by the selected force field.

There is a genuine interest in larger 1-decene oligomers for carbon dioxide thickening,[7] among other applications. We expand the calculations to larger molecules up to the 1-decene decamer. The chemical structures for all unsaturated oligomers are sketched in Figure 7.

For the 1-decene dimer, our results for shear viscosity are 3.28 ± 0.09 mPa·s at 40 °C and 1.19 ± 0.02 mPa·s at 100 °C, which agree with the experimental values:[27,45] 3.8 and 1.2 mPa·s, at 40 and 100 °C, respectively.

For the 1-decene dimer, trimer, and tetramer, experimental data of the kinematic viscosity are available.[46,47] Xue et al.,[47] based on the experimental data for the dimer, trimer, and the tetramer, proposed empirical correlations for the kinematic viscosity as a function of the oligomer molecular weight.

The viscosity index (VI), which is usually employed to characterize lubricants, is determined using the American Society for Testing and Materials standard method (ASTM D-2270),[48] which requires the kinematic viscosity at 40 and 100 °C. Most of the available experimental data are at the two temperatures.

The kinematic viscosity is computed as the ratio of the shear viscosity to the density. To compute the density, we use the last 500 ps of each NPT run and average over all independent trajectories. The density uncertainties are computed using the bootstrap method, and reported in Table S14. Figure 8 presents the kinematic viscosity of 1-decene oligomers (dimer,

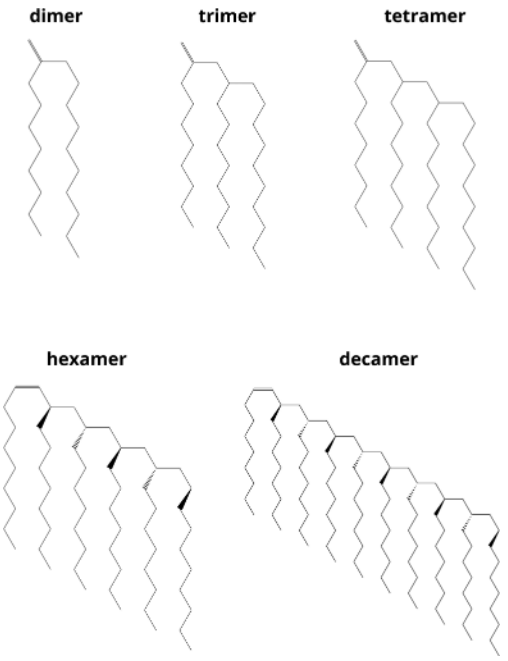

Figure 7. Chemical structures of 1-decene oligomers (dimer, trimer, tetramer, hexamer, and decamer).

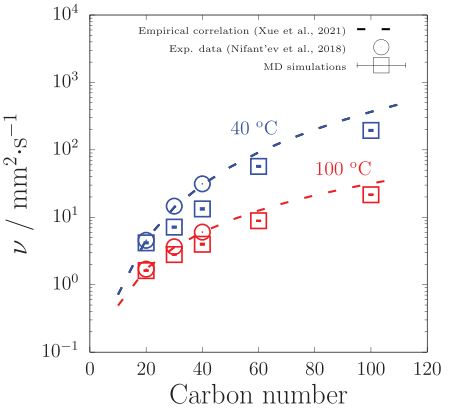

Figure 8. Kinematic viscosity of 1-decene oligomers versus carbon number. Blue circles, experimental data at 40 °C.[46] Blue dashed line, empirical correlation at 40 °C.[47] Blue squares, MD simulations with the L-OPLS-AA force field at 40 °C. Red circles, experimental data at 100 °C.[46] Red dashed line, empirical correlation at 100 °C.[47] Red squares are MD simulations with the L-OPLS-AA force field at 100 °C. The uncertainties of each point are reported in Table S20.

trimer, tetramer, hexamer, and decamer) at the two different temperatures, comparing the results from molecular dynamics simulations with the experimental data[46] and empirical correlations.[47] The overall agreement is good. The selected atomistic force field captures the general trend of kinematic viscosity with carbon number at the two temperatures.

CONCLUSIONS

We have demonstrated that two different methods to generate the traceless, symmetric pressure tensor, considered equivalent, provide different shear viscosities from the Green−Kubo formalism. One of the two methods is consistent, and the other can be modified by scaling the fluctuations of the diagonal components. Supercritical carbon dioxide, vapor and liquid *n*-pentane, and liquid *n*-decane shear viscosities are computed to

https://doi.org/10.1021/acs.jpcb.3c04994
J. Phys. Chem. B XXXX, XXX, XXX−XXX

illustrate the analysis between the two methods. Using a consistent method, we compute accurate kinematic viscosity for 1-decene oligomers (dimer, trimer, tetramer, hexamer, and decamer). We expect that our work paves the way for a more rigorous calculation of shear viscosity using equilibrium molecular dynamics.

■ ASSOCIATED CONTENT

Supporting Information

The Supporting Information is available free of charge at https://pubs.acs.org/doi/10.1021/acs.jpcb.3c04994.

Force field parameters for carbon dioxide, *n*-pentane, *n*-decane, 1-decene, and 1-decene oligomers; computed shear viscosity and its uncertainty for carbon dioxide at 308 K, *n*-pentane at 10 bar, and *n*-decane at 1 bar. computed density and shear viscosity, as well as their uncertainties, for 1-decene at 298.15 K and 1-decene oligomers at 1 bar; computed kinematic viscosity and its uncertainty for 1-decene oligomers at 1 bar (PDF)

■ AUTHOR INFORMATION

Corresponding Author

Luís Fernando Mercier Franco − *Universidade Estadual de Campinas, Campinas 13083-852, Brazil; Reservoir Engineering Research Institute, Palo Alto 94301 California, United States;* orcid.org/0000-0002-9334-9660; Email: lmfranco@unicamp.br

Author

Abbas Firoozabadi − *Reservoir Engineering Research Institute, Palo Alto 94301 California, United States; Chemical and Biomolecular Engineering, Rice University, Houston 77005 Texas, United States;* orcid.org/0000-0001-6102-9534

Complete contact information is available at: https://pubs.acs.org/10.1021/acs.jpcb.3c04994

Notes

The authors declare no competing financial interest.

■ ACKNOWLEDGMENTS

This work was made possible thanks to the Fulbright Program Junior Faculty Member Award and to São Paulo Research Foundation (FAPESP), grant #2018/02713-8. The authors also thank the John David Rogers Computing Center (CCJDR) at the Institute of Physics "Gleb Wataghin" of the University of Campinas for providing computational resources.

■ REFERENCES

(1) Bird, R. B.; Stewart, W. E.; Lightfoot, E. N. *Transport Phenomena*, 2nd ed.; John Wiley & Sons: New York, 2002; pp 11−15.

(2) Zhao, R.; Mi, P.; Xu, S.; Dong, S. Structure and properties of poly-α-olefins containing quaternary carbon centers. *ACS Omega* **2020**, *5*, 9142−9150.

(3) Rajewski, T. E.; Fokens, J. S.; Watson, M. C. The development and application of synthetic food grade lubricants. *Ind. Lubr. Tribol.* **2000**, *52*, 110−115.

(4) Ray, S.; Rao, P. V. C.; Choudary, N. V. Poly-α-olefin-based synthetic lubricants: a short review on various synthetic routes. *Lubr. Sci.* **2012**, *24*, 23−44.

(5) Santos, M. S.; Franco, L. F. M.; Castier, M.; Economou, I. G. Molecular dynamics simulation of *n*-alkanes and CO_2 confined by calcite nanopores. *Energy Fuels* **2018**, *32*, 1934−1941.

(6) Kar, T.; Firoozabadi, A. Effective viscosification of supercritical carbon dioxide by oligomers of 1-decene. *iScience* **2022**, *25*, 104266.

(7) Afra, S.; Alhosani, M.; Firoozabadi, A. Improvement in CO_2 geo-sequestration in saline aquifers by viscosification: from molecular scale to core scale. *Int. J. Greenh. Gas. Control.* **2023**, *125*, 103888.

(8) Goicochea, A. G.; Firoozabadi, A. CO_2 viscosification by functional molecules from mesoscale simulations. *J. Phys. Chem. C* **2019**, *123*, 29461−29467.

(9) Allen, M. P.; Tildesley, D. J. *Computer simulation of liquids*, 2nd ed.; Oxford Science Publications: New York, 2017; pp 74−75; 357−361.

(10) Green, M. S. Markoff Random Processes and the Statistical Mechanics of Time-Dependent Phenomena. II. Irreversible Processes in Fluids. *J. Chem. Phys.* **1954**, *22*, 398−413.

(11) Kubo, R. Statistical-Mechanical Theory of Irreversible Processes. I. General Theory and Simple Applications to Magnetic and Conduction Problems. *J. Phys. Soc. Jpn.* **1957**, *12*, 570−586.

(12) Helfand, E. Transport coefficients from dissipation in a canonical ensemble. *Phys. Rev.* **1960**, *119*, 1−9.

(13) Daivis, P. J.; Evans, D. J. Comparison of constant pressure and constant volume nonequilibrium simulations of sheared model decane. *J. Chem. Phys.* **1994**, *100*, 541−547.

(14) Chen, T.; Smit, B.; Bell, A. T. Are pressure fluctuation-based equilibrium methods really worse than nonequilibrium methods for calculating viscosities? *J. Chem. Phys.* **2009**, *131*, 246101.

(15) Borodin, O.; Smith, G. D.; Kim, H. Viscosity of a room temperature ionic liquid: predictions from nonequilibrium and equilibrium molecular dynamics simulations. *J. Phys. Chem. B* **2009**, *113*, 4771−4774.

(16) Maginn, E. J.; Messerly, R. A.; Carlson, D. J.; Roe, D. R.; Elliot, J. R. Best practices for computing transport properties 1.Self-diffusivity and viscosity from equilibrium molecular dynamics. *Living J. Comp. Mol. Sci.* **2020**, *1*, 6324.

(17) Jamali, S. H.; Wolff, L.; Becker, T. M.; de Groen, M.; Ramdin, M.; Hartkamp, R.; Bardow, A.; Vlugt, T. J. H.; Moultos, O. A. OCTP: a tool for on-the-fly calculation of transport properties of fluids with the order-*n* algorithm in LAMMPS. *J. Chem. Inf. Model.* **2019**, *59*, 1290−1294.

(18) Zhenyu, D.; Deng, S.; Zhao, L.; Nie, X.; Li, S.; Zhang, Y.; Zhao, J.; Zheng, N. Molecular dynamics study on viscosity coefficient of working fluid in supercritical CO_2 Brayton cycle: effect of trace gas. *J. CO2 Utilization* **2020**, *38*, 177−186.

(19) Sun, S.; Yang, Z.; Sheng, B.; Wang, Y.; Zhao, Y.; Dong, X.; Gong, M. The viscosity of liquid ethene: measurement and molecular dynamic simulation. *J. Chem. Thermodynamics* **2023**, *178*, 106957.

(20) Holian, B. L.; Evans, D. J. Shear viscosities away from the melting line: a comparison of equilibrium and nonequilibrium molecular dynamics. *J. Chem. Phys.* **1983**, *78*, 5147−5150.

(21) Rey-Castro, C.; Vega, L. F. Transport properties of the ionic liquid 1-ethyl-3-methylimidazolium chloride from equilibrium molecular dynamics simulation. The effect of temperature. *J. Phys. Chem. B* **2006**, *110*, 14426−14435.

(22) Bartolomeu, R. A. C.; Franco, L. F. M. Thermophysical properties of supercritical H_2 from molecular dynamics simulations. *Int. J. Hydrog. Energy* **2020**, *45*, 16372−16380.

(23) Potoff, J. J.; Siepmann, J. I. Vapor-liquid equilibria of mixtures containing alkanes, carbon dioxide, and nitrogen. *AIChE J.* **2001**, *47*, 1676−1682.

(24) Harris, J. G.; Yung, K. H. Carbon dioxide's liquid-vapor coexistence curve and critical properties as predicted by a simple molecular model. *J. Phys. Chem.* **1995**, *99*, 12021−12024.

(25) Aimoli, C. G.; Maginn, E. J.; Abreu, C. R. A. Transport properties of carbon dioxide and methane from molecular dynamics simulations. *J. Chem. Phys.* **2014**, *141*, 134101.

(26) Siu, S. W. I.; Pluhackova, K.; Böckmann, R. A. Optimization of the OLSA-AA force field for long hydrocarbons. *J. Chem. Theory Comput.* **2012**, *8*, 1459−1470.

(27) Mathas, D.; Holweger, W.; Wolf, M.; Bohnert, C.; Bakolas, V.; Procelewska, J.; Wang, L.; Bair, S.; Skylaris, C.-K. Evaluation of

methods for viscosity simulations of lubricants at different temperatures and pressures: a case study on PAO-2. *Tribol. Trans.* **2021**, *64*, 1138−1148.
(28) Schmitt, S.; Fleckenstein, F.; Hasse, H.; Stephan, S. Comparison of force fields for the prediction of thermophysical properties of long linear and branched alkanes. *J. Phys. Chem. B* **2023**, *127*, 1789−1802.
(29) Berendsen, H. J. C.; van der Spoel, D.; van Drunen, R. GROMACS: A message-passing parallel molecular dynamics implementation. *Comput. Phys. Commun.* **1995**, *91*, 43−56.
(30) Darden, T.; York, D.; Pedersen, L. Particle mesh Ewald: an *N* log(*N*) method for Ewald sums in large systems. *J. Chem. Phys.* **1993**, *98*, 10089−10092.
(31) Martínez, L.; Andrade, R.; Birgin, E. G.; Martínez, J. M. Packmol: A package for building initial configurations for molecular dynamics simulations. *J. Comput. Chem.* **2009**, *30*, 2157−2164.
(32) Berendsen, H. J. C.; Postma, J. P. M.; van Gunsteren, W. F.; DiNola, A.; Haak, J. R. Molecular-dynamics with coupling to an external bath. *J. Chem. Phys.* **1984**, *81*, 3684−3690.
(33) Nosé, S. A unified formulation of the constant temperature molecular-dynamics methods. *J. Chem. Phys.* **1984**, *81*, 511−519.
(34) Hoover, W. G. Canonical dynamics: Equilibrium phase-space distributions. *Phys. Rev. A* **1985**, *31*, 1695−1697.
(35) Grossfield, A.; Patrone, P. N.; Roe, D. R.; Schultz, A. J.; Siderius, D. W.; Zuckerman, D. M. Best practices for quantification of uncertainty and sampling quality in molecular simulations. *Living J. Comp. Mol. Sci.* **2019**, *1*, 5067.
(36) Hess, B. Determining the shear viscosity of model liquids from molecular dynamics simulations. *J. Chem. Phys.* **2002**, *116*, 209−217.
(37) Nelder, J. A.; Mead, R. A simplex method for function minimization. *Comput. J.* **1965**, *7*, 308−313.
(38) Zhang, Y.; Otani, A.; Maginn, E. J. Reliable viscosity calculation from equilibrium molecular dynamics simulations: a time decomposition method. *J. Chem. Theory Comput.* **2015**, *11*, 3537−3546.
(39) Lemmon, E. *Thermophysical properties of fluids*; CRC, 2009; p 1.
(40) Kioupis, L. I.; Maginn, E. J. Molecular simulation of poly-α-olefin synthetic lubricants: impact of molecular architeture on performance properties. *J. Phys. Chem. B* **1999**, *103*, 10781−10790.
(41) Kioupis, L. I.; Maginn, E. J. Impact of molecular architeture on the high-pressure rheology of hydrocarbon fluids. *J. Phys. Chem. B* **2000**, *104*, 7774−7783.
(42) Ravikumar, B.; Karathanassis, I. K.; Smith, T.; Gavaises, M. Dilute viscoelastic polymer solutions for dielectric heat transfer applications: a molecular dynamics study. *Int. J. Thermofluid.* **2023**, *18*, 100333.
(43) Nakamura, Y.; Hiraiwa, S.; Suzuki, F.; Matsui, M. High-pressure viscosity measurements of polyalphaolefins at elevated temperature. *Tribol. Online* **2016**, *2*, 444−449.
(44) Sagdeev, D. I.; Fomina, M. G.; Mukhamedzyanov, G. K.; Abdulagatov, I. M. Simultaneous measurements of the density and viscosity of 1-hexene + 1-decene mixtures at high temperatures and pressures. *J. Mol. Liq.* **2014**, *197*, 160−170.
(45) Bair, S. Pressure-viscosity response in the inlet zone for quantitative elastohydrodynamics. *Tribol. Int.* **2016**, *97*, 272−277.
(46) Nifant'ev, I. E.; Vinogradov, A. A.; Vinogradov, A. A.; Sedov, I. V.; Dorokhov, V. G.; Lyadov, A. S.; Ivchenko, P. V. Structurally uniform 1-hexene, 1-octene, and 1-decene oligomers: zirconocene/MAO-catalyzed preparation, characterization, and prospects of their use as low-viscosity low-temperature oil base stocks. *Appl. Catal. A-Gen.* **2018**, *549*, 40−50.
(47) Xue, J. Y.; Dong, S. W.; Mi, P. K.; Wang, L. B.; Wang, S. H.; Zhang, Z.; Zhang, Z. G.; Hu, J. S. Study of the structure-activity relationship of metallocene-catalysed poly-α-olefin (mPAO) base oil. *Mol. Syst. Des. Eng.* **2021**, *6*, 722−729.
(48) Standard practice for calculating viscosity index from kinematic viscosity at 40 and 100 °C; *ASTM D2270-10*, ASTM, 2016.

https://doi.org/10.1021/acs.jpcb.3c04994
J. Phys. Chem. B XXXX, XXX, XXX−XXX